Research Article Vol. 58, No. 13 / 1 May 2019 / Applied Optics D61

applied optics

Wavefront shaping optical elements recorded in photo-thermo-refractive glass

Ivan Divliansky,[1,*] Fedor Kompan,[1] Evan Hale,[1] Marc Segall,[2] Axel Schülzgen,[1] and Leonid B. Glebov[1]

[1]CREOL, College of Optics and Photonics, University of Central Florida, 4304 Scorpius St., Orlando, Florida 32816, USA
[2]C2 Intellisense Systems Inc., 20600 Gramercy Place, Torrance, California 90501, USA
*Corresponding author: ibd1@creol.ucf.edu

Received 17 December 2018; revised 12 March 2019; accepted 14 March 2019; posted 14 March 2019 (Doc. ID 355481); published 9 April 2019

The paper presents an overview of the benefits of recording phase masks into the bulk of photo-thermo-refractive glass. We demonstrate that both binary and gray-scale phase masks can be encoded into the medium, and that such masks can be used for mode conversion and beam shaping with near-theoretical efficiency. We further demonstrate that by encoding the phase mask profile into a transmitting volume Bragg grating, it is possible to create tunable and achromatic phase masks without requiring a complex phase pattern.

https://doi.org/10.1364/AO.58.000D61

1. INTRODUCTION

Phase masks that provide a predetermined profile of phase retardation across the aperture of optical beams are an efficient method for beam control and shaping (see, e.g., [1–3]), beams-splitting, coronagraphy [4–6], and in general a way to fabricate diffractive optics used in a broad spectrum of applications [7]. It is known that phase can be controlled either by varying the physical thickness or the local refractive index of a plane parallel plate, and multiple authors describe the methods necessary to create either binary or multilevel phase elements [7–9]. Conventional methods of such optical element fabrication are typically based on spatially selective etching or deposition [1–6]. However, one of the main drawbacks of such techniques is that these elements are very sensitive to their working condition (dust, humidity, etc.) as the phase profile is controlled by very shallow grooves. With the development of new photosensitive media, it becomes possible to spatially control the local refractive index and therefore to record similar phase plates without changing the local physical thickness of the plate. One of the most advanced photosensitive materials is photo-thermo-refractive (PTR) glass. PTR glass exhibits refractive index change after successive exposure to ionizing radiation and thermal treatment at temperatures above the glass transition temperature and is commercially used for the recording of diffractive holographic elements (volume Bragg gratings) [10] and refractive elements (Fresnel lenses) [11]. The main features of these optical elements are their low absorption and scattering in the visible and near IR spectral range and their high laser induced damage threshold, which make them very suitable in high power laser applications [12,13]. In this paper, we present an overview of different wavefront shaping elements recorded in PTR glass and their recording techniques. The paper begins with the description of the contact copy technique in application for fabrication of permanent binary phase masks with high tolerance to laser radiation [14]. Implementation of an imaging technique based on a digital micromirror device significantly extends capabilities and the functionality of the phase masks recording technique, making it possible to produce phase masks with arbitrary gray-scale phase profiles [15]. It is then demonstrated how the phase profiles can be encoded into a volume Bragg grating resulting in spectrally tunable phase masks whose operation wavelength can be adjusted by tuning the incident angle [16]. Finally, it is shown how holographic phase masks can be incorporated into an achromatic optical system capable of performing mode conversion of broadband sources such as femtosecond lasers [17].

2. BINARY PHASE MASKS

One common use for phase masks is conversion between different beam profiles. In particular, let us consider methods for converting a Gaussian beam into a higher order TEM_{mn} or LG_{mn} mode. Transforming a Gaussian beam into higher order modes can be achieved with 100% conversion efficiency using an interferometric arrangement [18], but this can be time-consuming to align and is sensitive to vibrations. Transformation into the TEM_{11} mode or LG_{04} mode can also be achieved using binary phase masks containing either four or eight sectors in an azimuthal pattern, respectively, with each sector having a phase incursion shifted by π relative to the phase incursion of the adjacent sectors (Fig. 1) [4–6].

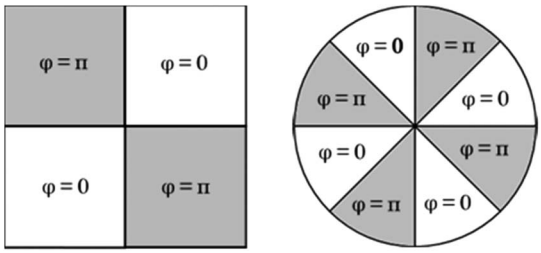

Fig. 1. Phase profile for (a) four-sector and (b) eight-sector binary phase masks for Gaussian beam transformation to TEM_{11} and LG_{04} modes, respectively.

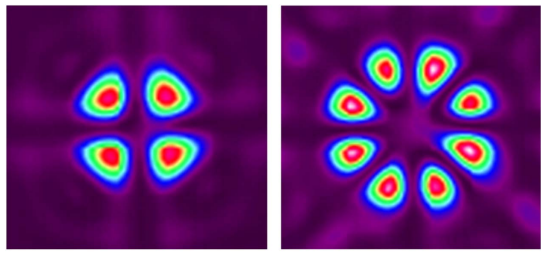

Fig. 3. Experimental far field intensity profile produced by the (a) four-sector and (b) eight-sector VPM.

While all previous demonstrations of such binary masks have been carried out by local modification of the sample's thickness, we will consider in this paper mode convertors based on volume phase masks (VPMs) where phase incursion is produced by local variations of refractive index [14].

A Gaussian beam passing through the centers of such VPMs will have a far field intensity distribution as shown in Fig. 2. The distribution of energy, however, may not be similar to the higher order mode of the same width as the Gaussian beam, since the bucket for a higher order mode is much larger than the bucket for a Gaussian beam. Therefore, it is evident that the width w of the mode in question may not be equal to the width u_0 of the incident beam for optimal conversion, and thus the efficiency should be defined in terms of the relative widths:

$$\eta(w,u_0)=\frac{|\iint E^*_{nm}(w)E_{00}(u_0)T\,\mathrm{d}A|^2}{\iint |E_{nm}(w)|^2\mathrm{d}A\cdot\iint |E_{00}(u_0)T|^2\mathrm{d}A}. \quad (1)$$

Here T is the transmittance function of the phase mask. For a given incident beam width u_0, calculations indicate that the maximum conversion efficiency of the four sector VPM into the TEM_{11} mode is 68.4% (when $w/u_0=0.577$) and the maximum efficiency of the eight sector VPM into the LG_{04} mode is 29% (when $w/u_0=0.445$).

In order to validate this model we fabricated two phase masks in 25 mm × 25 mm PTR glass plates using the contact copying technique and binary amplitude master masks. A master binary amplitude mask was first recorded lithographically in a fused silica plate for each pattern. This mask permitted selective exposure of the PTR glass with the designed profiles, in order to achieve a lower refractive index only in the UV-exposed regions. The PTR plate was then placed in contact with the master mask having matching fluid in between them and homogeneously exposed to UV radiation from a He–Cd laser at 325 nm with a dosage of 1 J/cm^2. The samples were then developed at a temperature of ~520°C.

As the total phase incursion is given by

$$\varphi=\frac{2\pi\Delta nL}{\lambda}, \quad (2)$$

the plates were subsequently polished down to a given thickness L in order to secure a π phase shift between the unexposed and the exposed regions at $\lambda=633$ nm. It should be noted that during recording there is diffraction of the UV beam at the edges of the amplitude mask. This results in a transition region of approximately 6 μm width between the sectors, which has a negligible effect on the conversion efficiency.

The phase masks were placed in a collimated single mode beam from a He–Ne laser emitting at 633 nm with a Gaussian intensity distribution, and the intensity distribution of the transmitted beam was characterized in the focal plane of a lens (Fig. 3). Excellent agreement with the theoretical intensity distribution can be observed.

The results show that volume phase masks with plane parallel polished surfaces recorded in PTR glass are elements capable of controlling the intensity profile of laser beams. The two examples demonstrated partial conversion of a Gaussian beam to the TEM_{11} mode or the LG_{04} mode with near-theoretical profiles. These phase masks are very robust (the element is written within the volume of the robust glass plate and cannot be deleted or altered) and are highly suitable to high power and high energy (CW or pulsed) applications. Further, the refractive index change can be adjusted as necessary for use at any wavelength.

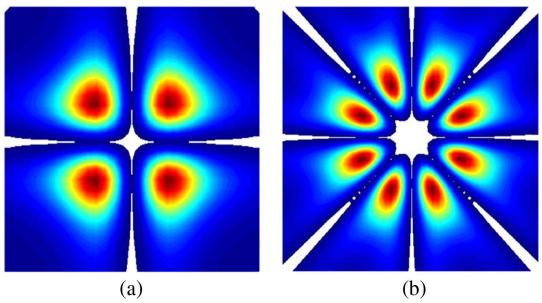

Fig. 2. Theoretical far field intensity profile produced by the (a) four-sector and (b) eight-sector VPM.

3. GRAY-SCALE PHASE MASKS

While the binary phase masks described above are capable of beam shaping, their binary nature limits the maximum conversion efficiency possible. This can be surmounted by using gray-scale phase masks instead of binary masks. A gray-scale phase mask can have any phase variation from 0 to 2π. Production of phase masks with gray levels using the contact-copy method is considerably more challenging than binary masks and, hence, comes at excessive cost. For that reason, the phase variation in greyscale masks is more often created by varying the thickness of the mask while keeping the refractive index change uniform

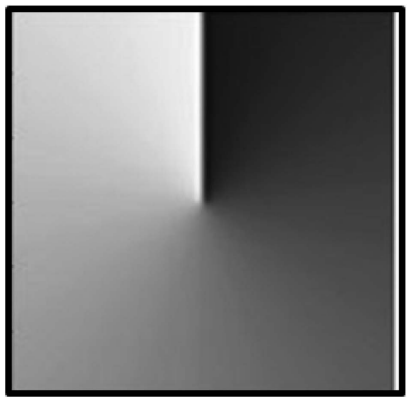

Fig. 4. Example of a phase incursion profile for a gray-scale vortex phase mask.

across the mask. Phase masks of that type are typically fabricated by etching and deposition techniques in glass or polymer. An example of a common phase mask of that type is a plate with the thickness of the plate varying in a spiral pattern, which introduces a helical phase profile in a beam upon passing through it (Fig. 4). Phase masks with variable thickness fabricated in glass are more durable than their counterparts produced by refractive index change in polymers. However, the fabrication process is very time consuming and cost intensive since thickness of the plate in each segment has to be maintained with high accuracy to ensure that no aberrations are introduced into the beam during beam shaping [19,20].

In this part of the paper, we present a new method for recording gray level phase patterns inside PTR glass [15]. It provides a relatively inexpensive and durable solution for wavefront shaping of laser beams, including high power beams. The method employs a digital micromirror device (DMD) for generation of an amplitude pattern, which is then transformed into the corresponding phase pattern by being recorded into a volume of a photosensitive PTR glass. The subsequently created phase mask can be placed into a laser beam path for beam shaping and mode conversion.

The DMD device is a micro-opto-electromechanical system that contains a rectangular array of micrometer-sized mirrors that can be individually controlled to provide tilt to specific angles (−12° or +12° for our chosen DMD), corresponding to "off" and "on" states, respectively [21]. Applying voltage to individual mirrors will set the mirrors into "on" position, and therefore, a spatial pattern of high complexity can be achieved. This pattern is then imaged into a slab of photosensitive material. The areas corresponding to mirrors in the "on" position will be exposed, and those areas will obtain a refractive index change with respect to unexposed areas, thus creating a certain phase shift. Grey-scale phase patterns can be created as well by varying the total duration of the target mirror being in the "on" position, thus enabling a controllable illumination dosage and therefore any value of phase shift between 0 and 2π in the photosensitive medium. The ultimate complexity of the pattern is only limited by its highest spatial frequency, which is determined by the resolution of the DMD and of the holographic material.

The main advantage of this recording technique can be demonstrated by creating a gray-scale phase mask such as a vortex phase mask. The designed 14-step phase profile of the vortex phase mask is shown in Fig. 5. The phase undergoes a linear change from 0 to 2π in an azimuthal profile around the mask. This phase mask can be used to convert a Gaussian beam into a helical Laguerre–Gaussian beam of the first order LG_{01} with an optical vortex in the middle. The spatial phase profile of an actual vortex phase mask created using the recording system and measured with a Zygo interferometer is shown in Fig. 5(b). Black areas in the spatial phase profile are the result of a sharp refractive index gradient that could not be processed by the used interferometer. The phase profile shown in the figure corresponds to the mask fabricated to work at 633 nm with thickness of 1.1 mm and 575 ppm refractive index difference at the 2π-phase shift boundary. It can be seen that the mask demonstrates successful conversion of a Gaussian beam to the LG_{01} mode. The resulting ring shape intensity profile is shown in Fig. 5(d), and it resembles the theoretically predicted far field profile [Fig. 5(c)]. Figure 5(e) demonstrates an LG_{01} mode generated from a Gaussian beam by means of a similar mask produced for operation at 1064 nm.

The vortex phase mask demonstrated above is an illustrative example of the capabilities of gray-scale phase masks in PTR glass for beam shaping and mode conversion, but it is far from the only possible profile. Beams of many other profiles can be generated using a corresponding phase mask design, be it a binary mask, multilevel, or smooth and continuous mask.

In conclusion, we have shown here that it is possible to record gray-scale phase profiles as well as binary profiles into PTR glass. The production of such masks is more cost-efficient compared to phase plates produced by surface processing, and it allows PTR-based masks to be used for virtually any phase pattern, which in turn can be used to generate a wide range of optical beam profiles.

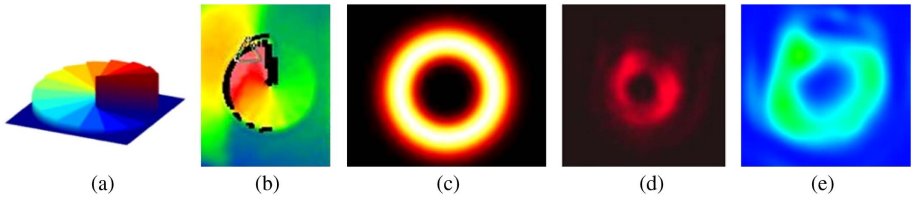

Fig. 5. Vortex phase mask with (a) target phase profile, (b) measured phase profile, (c) ideal mode conversion, (d) measured mode conversion at 633 nm, (e) measured mode conversion by another mask at 1064 nm.

4. HOLOGRAPHIC PHASE MASKS

The advantages of using phase masks recorded into the bulk of PTR glass can be further enhanced by encoding the phase mask profile into holograms. Here we present a method to create spectrally tunable phase masks by encoding phase profiles into volume Bragg gratings, allowing these holographic elements to be used as phase masks at any wavelength capable of satisfying the Bragg condition of the hologram [16]. Moreover, this approach enables the capability to encode and multiplex several phase masks into a single holographic element without cross talk while maintaining high diffraction efficiency. As examples, we demonstrate fiber mode conversion with near-theoretical conversion efficiency as well as simultaneous mode conversion and beam combining at wavelengths far from the original hologram recording wavelength.

As described earlier, phase masks, whether conventionally fabricated or recorded in the bulk of a photosensitive medium, are capable of inducing arbitrary beam shaping to an incident beam. However, because the phase shift is induced by changing the local optical path length (whether by refractive index change or geometrical path length change) these phase masks are inherently limited to use at a specific wavelength, which limits the range of potential applications. To increase this range, achromatic phase masks have been previously produced utilizing either birefringent materials or the birefringence in diffraction gratings with periods below the working wavelength [22,23]. Other techniques include wavelength multiplexing several computer-generated holograms so that arbitrary wavefronts can be generated when illuminated by the appropriate wavelength beam [24–26]. This technique allows the diffracted beam to have the same wavefront for multiple incident wavelengths but requires that a separate hologram be recorded for each desired wavelength. Therefore, to make this a truly achromatic device many holograms must be recorded, and the diffraction efficiency of each hologram will necessarily be reduced.

We have developed a new approach where a tunable element can be generated by encoding predetermined phase mask profiles [14] into transmitting volume Bragg gratings (TBGs) [27,28], which produce holographic phase masks (HPMs). Though this technique has been demonstrated for HPMs utilized at reconstruction wavelengths identical to the recording wavelength [29,30], we show that HPMs can produce identical diffracted phase profiles over a wide range of wavelengths as long as the Bragg condition of the volume grating is satisfied [16]. This is in contrast to more complex holograms where, though they can be read at any wavelength satisfying the Bragg condition, generally cannot reconstruct the same phase profile at wavelengths different than the recording one. The HPM utilizes the diffraction characteristics of TBGs, which can diffract up to 100% of a beam into a single order and can diffract over a broad range of wavelengths by changing the angle of incidence (with the diffraction efficiency depending on the wavelength and strength of the grating) [23]. The high angular selectivity of a TBG also allows for several TBGs to be multiplexed into the same element with little to no cross talk between gratings; each grating is accessed by altering the beam's angle of incidence onto the element. To simplify fabrication and to provide a clear demonstration of the phenomenon, we chose to use binary phase profiles, but the approach is fully applicable for multilevel phase masks as well.

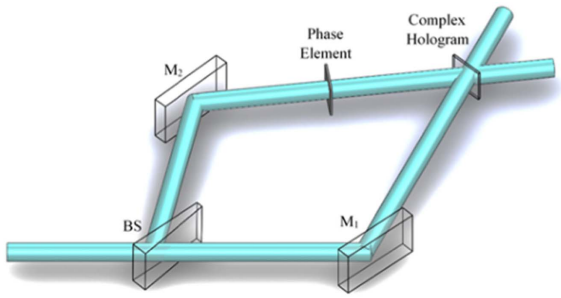

Fig. 6. Experimental setup for holographic recording of a phase mask encoded in a transmitting volume Bragg grating. BS, beamsplitter; M_1 and M_2, mirrors.

To encode the phase profile into a TBG, consider the holographic recording setup in Fig. 6. Here a multilevel phase mask has been placed into one arm of a two-beam interference system (the object beam), where the two beams interfere at an angle θ relative to the normal of the holographic sample. If the thickness of the sample, the axial distance between the phase mask and the sample, and θ are small, then the phase profile recorded in the hologram will be approximately the same as that of the original phase mask. The recorded hologram will have a refractive index profile of

$$n(x,y,z) = n_0 + n_1 \cos(\vec{K}\cdot\vec{r} + \varphi(x,y)), \tag{3}$$

where n_0 is the background refractive index, n_1 is the refractive index modulation, and $\vec{K} = \vec{k}_1 - \vec{k}_2$ is the grating vector. Once the hologram is recorded, it is placed in a system with some probe beam to be diffracted, which may or may not have the same wavelength as the recording beams.

In order to directly and accurately compare the diffraction efficiency of the HPM with that of a standard TBG, we fabricated a sample containing both an HPM and a homogeneous TBG in the same volume of PTR glass. This was done by recording an HPM and then removing the phase mask from the object beam and rotating the PTR glass sample without lateral shifting to record a tilted TBG with the same recording dosage. Recording both elements in the same volume ensured that the local refractive index change and any sample inhomogeneities would be shared between the elements and demonstrated a new opportunity for holographic phase mask multiplexing. As shown in Fig. 7, the diffraction efficiencies of each element are approximately the same, showing good agreement with theoretical predictions. Note also that there is no cross talk between the two multiplexed holograms, demonstrating that the HPM preserves the narrow angular acceptance of standard TBGs.

As demonstrated previously, a four-sector binary phase mask can itself be used as a partial optical mode converter when the probe beam center is properly aligned with respect to the phase steps. Such a binary phase mask, though, works only for the particular wavelength for which the phase shift is π. As shown in Fig. 2(a), the expected far field intensity profile for a beam passing through the center of a four-sector regular binary phase

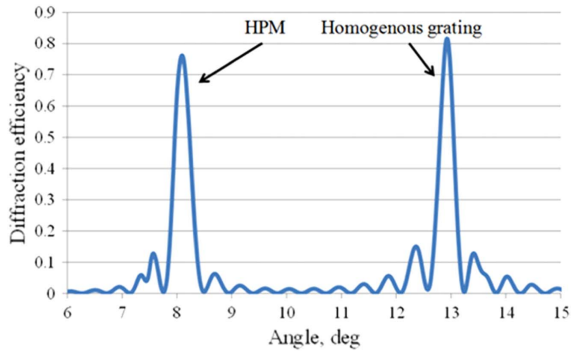

Fig. 7. Diffraction efficiency angular spectrum of an HPM and a homogenous grating.

mask consists of a four-lobed clover pattern, indicating partial conversion to the TEM_{11} mode. However, effective mode conversion only occurs at the design wavelength. Similar mode conversion results have been recently demonstrated for fiber modes [31]. To demonstrate the capabilities of HPMs we encoded such a four sector binary phase mask in a TBG. If the encoded binary phase steps are indeed transferred to the probe beams diffracted from the HPM at their respective Bragg wavelengths, the HPM should simultaneously act as a diffraction element and a mode converter when the beams are correctly aligned to the phase steps. Three beams (3 mm in diameter at $1/e^2$) at wavelengths in the visible and the infrared regions were applied to study the wavelength dependence of diffraction and mode conversion using the HPM.

As shown in Figs. 8(b)–8(d), for the three very different Bragg wavelengths (632.8, 975, and 1064 nm), the diffracted beam profiles exhibited the predicted four-lobed pattern.

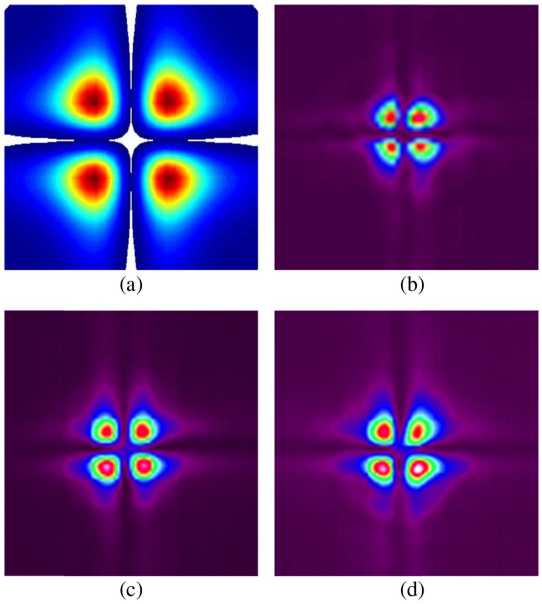

Fig. 8. (a) Simulated far field profile of a beam after passing through an ideal four-sector binary mask and the diffracted beam from a four-sector HPM at (b) 632.8 nm, (c) 975 nm, and (d) 1064 nm. The sizes shown here are not to scale.

This clearly confirms our initial thesis that the phase profile is being preserved in the diffracted order for an extremely broad range of wavelengths. Thus, contrary to conventional phase masks, holographic phase masks are tunable in a wide spectral range.

5. ACHROMATIC PHASE MASKS

In this last section of the paper we further extend the capabilities of HPMs by presenting an achromatic optical system capable of performing laser mode conversion over a wide spectral range of 1 μm. The system builds upon the holographic mode conversion elements described in the previous section and consists of an HPM element inserted between two surface gratings, allowing any wavelength to satisfy the Bragg condition of the phase mask without the need for angular tuning.

True achromatization of HPMs can be achieved by pairing the Bragg grating with two surface gratings [32]. According to coupled wave theory [27], incident light onto a TBG undergoes diffraction under the Bragg condition,

$$2\Lambda_{\mathrm{VBG}} \sin \theta_B = \lambda, \tag{4}$$

where Λ_{VBG} is the TBG's grating period, θ_B is the Bragg angle, and λ is the incident wavelength. A TBG's Bragg condition is similar to the dispersion equation for a surface grating:

$$\Lambda_{\mathrm{SG}} \sin \theta = m\lambda. \tag{5}$$

Here Λ_{SG} is the period of the surface grating, θ is the diffracted angle, and m is the order of diffraction. When the two gratings periods satisfy the condition $2\Lambda_{\mathrm{TBG}} = \Lambda_{\mathrm{SG}}$, the first order diffracted angle from the surface grating will match the Bragg condition for the TBG for all wavelengths. This circumvents the broad but still finite spectral selectivity of the TBG and results in increased diffracted spectral bandwidth and overall diffraction efficiency for sources with a bandwidth larger than the TBG's spectral selectivity. Although using surface gratings with twice the period of the TBG's period is ideal, gratings with periods in close proximity have also been shown to be effective [33].

The proposed system of the two surface gratings and the holographic phase mask is laid out in Fig. 9 [17]. Here the broadband input is diffracted through the first surface grating, where the diffracted angle for each spectral component is equal to the Bragg angle of the TBG.

With this configuration, the TBG's spectral bandwidth acceptance is highly dependent on the spectral diffraction properties of the surface grating chosen. After pairing with the first surface grating, the total spectral bandwidth of the two elements will equal the bandwidth of the surface grating, simulated to be ~750 nm (FWHM). This combination of surface and volume gratings with periods' ratio of 2 to 1 results in a 30 times improvement for the theoretical spectral bandwidth (FWHM). The TBG paired with one surface grating, however, does not remove the angular chromatic dispersion introduced by the surface grating. This chromatic dispersion limits the actual bandwidth of the system to a couple of nanometers for applications needing minimal chromatic aberrations, such as mode conversion. Simply, adding a second identical surface grating after the TBG eliminates the angular dispersion, allowing the full theoretical bandwidth of 750 nm (FWHM) to be

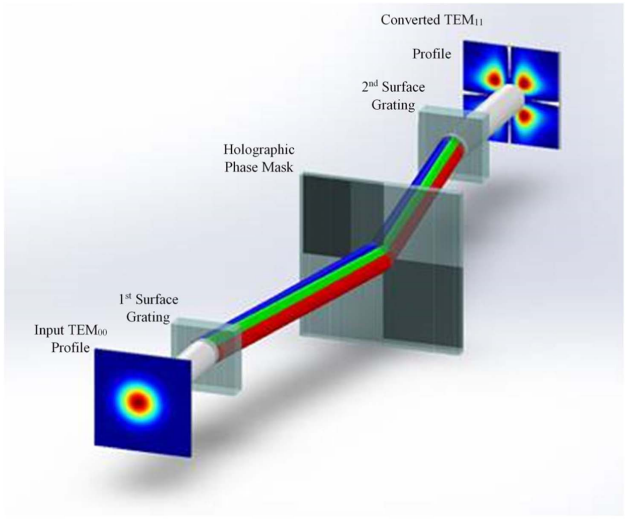

Fig. 9. Concept of an achromatic holographic phase mask using a combination of two surface gratings with a tunable holographic phase mask placed between them.

collinear, vastly improving the achromaticity of the system from a few nanometers to several hundreds of nanometers. When replacing the TBG with an HPM, which has the same diffraction properties as a simple TBG, the resulting system becomes an achromatic HPM (AHPM).

To experimentally demonstrate the potential applications of the AHPM, a mode converter using a four-sector binary HPM was setup. The goal was to achieve successful mode conversion from a fundamental TEM_{00} to a TEM_{11} mode profile for laser sources of different wavelengths without needing to angularly tune the HPM.

In the experiment five different narrow linewidth laser sources were used in order to cover a wavelength range of over 1 μm (488–1550 nm). Commercial Argon–ion (488 nm), He–Ne (543 and 632 nm), and diode (765, 1064, and 1550 nm) laser sources were used to show the achromatic properties of the AHPM. Successful TEM_{00} to TEM_{11} mode conversion was achieved for each source, as shown in Fig. 10.

Ultrafast femtosecond laser systems have enabled many breakthroughs in the fields of science and technology, and currently extensive research is being done in manipulating the transverse mode structure of such systems in order to further their applicability [34]. As an example, the zero-intensity center of higher order transverse modes provides an optical trapping effect for a wide range of potential applications in subwavelength nonlinear microscopy [35], optical tweezers for micro- and nanomanipulation [36], and for creating filamentation of radiation [37,38]. After the demonstration of the broadband properties of AHPMs, it is obvious that they can be used in creating such non-Gaussian beam profiles where broadband laser sources are used. Using a commercial femtosecond laser system (FemtoFErb 780 from Toptica Photonics, Inc), showed the true potential of the HPMs in manipulating the wavefront of broadband laser sources. Figure 11 shows the mode transformations of the femtosecond beam (TEM_{00} to TEM_{01}, TEM_{10}, and TEM_{11}) using the AHPM system.

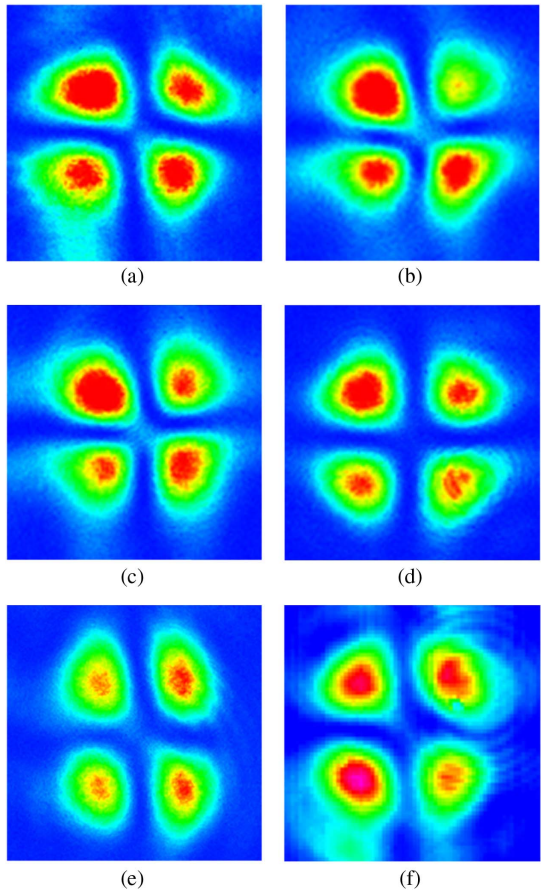

Fig. 10. Far field profiles of the TEM_{11} mode converted outputs for an (a) 488 nm, (b) 543 nm, (c) 632 nm, and (d) 765 nm diode; (e) 1064 nm, and (f) 1550 nm laser (sizes are not to scale).

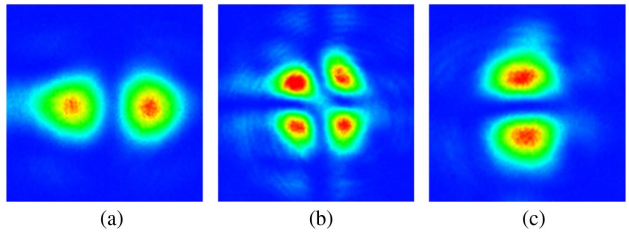

Fig. 11. Far field intensity profiles of femtosecond pulse Gaussian mode conversion to (a) TEM_{10}, (b) TEM_{11}, and (c) TEM_{01} after passing through the AHPM (sizes are not to scale).

The measurements of the spectrum of the beam after the AHPM showed negligible alteration to the spectral structure, confirming that broadband mode conversion is achievable when using an AHPM system.

In conclusion, the pairing of an HPM with surface gratings having twice its period to create an achromatic element functioning as a phase mask for broadband sources was demonstrated. These AHPMs may be used to simultaneously diffract and convert transverse laser modes. This new optical element dramatically increases the potential applications of optical phase masks in broadband sources.

6. CONCLUSIONS

In this paper we have summarized the potential for encoding phase masks into the bulk of PTR glass. Both binary and gray-scale phase profiles can be encoded, and the phase profiles discussed here can all be used for beam shaping and mode conversion with near-theoretical efficiency. Furthermore, arbitrary phase profiles can also be encoded into TBGs to form HPMs that, through the use of angular tuning, significantly extend the wavelength range that the phase mask can be used over. By matching the HPM to surface gratings of the appropriate grating period, it is possible to make a truly achromatic phase mask, with no angular tuning required and no complex phase profiles necessary. These capabilities, coupled with the advantages of recording in the bulk photosensitive glass rather than surface processing, offer the potential to significantly extend the uses of phase masks, such as use in high power applications, while minimizing overall cost, as it is no longer necessary to create separate phase masks for all desired wavelengths.

REFERENCES

1. N. Stelmakh, "Harnessing multimode broad-area laser-diode emission into a single-lobe diffraction-limited spot," IEEE Photon. Technol. Lett. **19**, 1392–1394 (2007).
2. M. Wang, C. Yu, and A. Varela, "Efficient pseudo-nondiffracting beam shaping using a quasicontinuous-phase diffractive element," Opt. Eng. **40**, 517–524 (2001).
3. W. Mohammed, M. Pitchumani, A. Mehta, and E. Johnson, "Selective excitation of the LP11 mode in step index fiber using a phase mask," Opt. Eng. **45**, 074602 (2006).
4. F. Lemarquis, M. Lequime, G. Albrand, L. Escoubas, J. Simon, J. Baudrand, P. Riaud, D. Rouan, A. Boccaletti, P. Baudoz, and D. Mawet, "Manufacturing of 4-quadrant phase mask for nulling interferometry in thermal infrared," Proc. SPIE **5250**, 435–443 (2004).
5. D. Rouan, P. Riaud, A. Boccaletti, Y. Clénet, and A. Labeyrie, "The four-quadrant phase-mask coronagraph. I. Principle," Publ. Astron. Soc. Pac. **112**, 1479–1486 (2000).
6. N. Murakami, J. Nishikawa, K. Yokochi, M. Tamura, N. Baba, and L. Abe, "Achromatic eight-octant phase-mask coronagraph using photonic crystal," Astrophys. J. **714**, 772–777 (2010).
7. J. Turunen and F. Wyrowski, eds., *Diffractive Optics for Industrial and Commercial Applications* (Akademie, 1997).
8. V. A. Soifer, *Diffractive Optics and Nanophotonics* (CRC Press, 2017).
9. V. A. Soifer, *Computer Design of Diffractive Optics* (Cambridge International Science/Woodhead Publishing, 2013).
10. L. B. Glebov, "Volume hologram recording in inorganic glasses," Glass Sci. Technol. **75**, 73–90 (2002).
11. L. Siiman, J. Lumeau, and L. Glebov, "Phase Fresnel lens recorded in photo-thermo-refractive glass by selective exposure to infrared ultrashort laser pulses," Opt. Lett. **34**, 40–42 (2009).
12. L. Glebov, "Volume holographic elements in a photo-thermo-refractive glass," J. Hologr. Speckle **5**, 77–84 (2008).
13. J. Lumeau, L. Glebova, and L. Glebov, "Near-IR absorption in high purity photothermorefractive glass and holographic optical elements: measurement and application for high-energy lasers," Appl. Opt. **50**, 5905–5911 (2011).
14. M. SeGall, V. Rotar, J. Lumeau, S. Mokhov, B. Zeldovich, and L. B. Glebov, "Binary volume phase masks in photo-thermo-refractive glass," Opt. Lett. **37**, 1190–1192 (2012).
15. F. Kompan, D. Nguyen, Z. Labossiere, D. Guacaneme, I. Divliansky, A. Schülzgen, and L. Glebov, "Beam shaping holographic optical elements recorded in PTR glass using a digital micro-mirror device," (to be published).
16. M. SeGall, I. Divliansky, C. Jollivet, A. Schülzgen, and L. B. Glebov, "Holographically encoded volume phase masks," Opt. Eng. **54**, 076104 (2015).
17. I. Divliansky, E. R. Hale, M. SeGall, and L. B. Glebov, "Achromatic complex holograms for laser mode conversion," Opt. Express **27**, 225–239 (2019).
18. G. Machavariani, A. Ishaaya, L. Shimshi, N. Davidson, A. Friesem, and E. Hasman, "Efficient mode transformations of degenerate Laguerre-Gaussian beams," Appl. Opt. **43**, 2561–2567 (2004).
19. C. Dorrer, "High-damage-threshold beam shaping using binary phase plates," Opt. Lett. **34**, 2330–2332 (2009).
20. C. Rotschild, S. Zommer, S. Moed, O. Hershcovitz, and S. G. Lipso, "Adjustable spiral phase plate," Appl. Opt. **43**, 2397–2399 (2004).
21. D. Dudley, W. M. Duncan, and J. Slaughter, "Emerging digital micromirror device (DMD) applications," Proc. SPIE **4985**, 14 (2003).
22. M. Bass, *Handbook of Optics*, 2nd ed. (McGraw-Hill, 1994), Vol. **2**.
23. D. Mawet, C. Lenaerts, V. Moreau, Y. Renotte, D. Rouan, and J. Surdej, "Achromatic four quadrant phase mask coronagraph using the dispersion of form birefringence," in *Astronomy with High Contrast Imaging*, C. Aime and R. Soummer, eds. (Cambridge University, 2003).
24. J. Rosen, M. Segev, and A. Yariv, "Wavelength-multiplexed computer-generated volume holography," Opt. Lett. **18**, 744–746 (1993).
25. G. A. Rakuljic, V. Leyva, and A. Yariv, "Optical data storage by using orthogonal wavelength-multiplexed volume holograms," Opt. Lett. **17**, 1471–1473 (1992).
26. T. D. Gerke and R. Piestun, "Aperiodic volume optics," Nat. Photonics **4**, 188–193 (2010).
27. H. Kogelnik, "Coupled wave theory for thick volume holograms," Bell Syst. Tech. J. **48**, 2909–2947 (1969).
28. I. Ciapurin, L. Glebov, and V. Smirnov, "Spectral combining of high-power fiber laser beams using Bragg grating in PTR glass," Proc. SPIE **5335**, 116 (2004).
29. K. Aoki, A. Okamoto, Y. Wakayama, A. Tomita, and S. Honma, "Selective multimode excitation using volume holographic mode multiplexer," Opt. Lett. **38**, 769–771 (2013).
30. Y. Wakayama, A. Okamoto, K. Kawabata, A. Tomita, and K. Sato, "Mode demultiplexer using angularly multiplexed volume holograms," Opt. Express **21**, 12920–12933 (2013).
31. K. Igarashi, D. Souma, T. Tsuritani, and I. Morita, "Performance evaluation of selective mode conversion based on phase plates for a 10-mode fiber," Opt. Express **22**, 20881–20893 (2014).
32. L. Glebov, V. Smirnov, N. Tabirian, and B. Zeldovich, "Implementation of 3D angular selective achromatic diffraction optical grating device," in *Frontier in Optics* (OSA, 2003), paper WW3.
33. S. Wu, X. Yuan, X. Zhang, J. Feng, K. Zou, and G. Zhang, "Broadband angular filtering with a volume Bragg grating and a surface grating pair," Opt. Lett. **39**, 4068–4071 (2014).
34. Z. Qiao, L. Kong, G. Xie, Z. Qin, P. Yuan, L. Qian, X. Xu, J. Xu, and D. Fan, "Ultraclean femtosecond vortices from a tunable high-order transverse-mode femtosecond laser," Opt. Lett. **42**, 2547–2550 (2017).
35. N. Tian, L. Fu, and M. Gu, "Resolution and contrast enhancement of subtractive second harmonic generation microscopy with a circularly polarized vortex beam," Sci. Rep. **5**, 13580 (2015).
36. C. Liu, Z. Guo, Y. Li, X. Wang, and S. Qu, "Manipulating ellipsoidal micro-particles by femtosecond vortex tweezers," J. Opt. **17**, 035402 (2015).
37. N. Jhajj, E. W. Rosenthal, R. Birnbaum, J. K. Wahlstrand, and H. M. Milchberg, "Demonstration of long-lived high-power optical waveguides in air," Phys. Rev. X **4**, 011027 (2014).
38. M. Alshershby, Z. Hao, and J. Lin, "Guiding microwave radiation using laser-induced filaments: the hollow conducting waveguide concept," J. Phys. D **45**, 265401 (2012).